A voltage tunable quantum dot photodetector for terahertz detection

A voltage tunable quantum dot photodetector for terahertz detection

Wei Wu, Dibyendu Dey and Hooman Mohseni

Bio-inspired Sensors and Optoelectronics Laboratory (BISOL), Department of Electrical Engineering and Computer Science, Northwestern University, Evanston IL 60208, USA

E-mail: wwu@u.northwestern.edu and hmohseni@ece.northwestern.edu

Abstract
A voltage tunable quantum dot (QD) photodetector for terahertz detection based on intersublevel transitions is proposed. The intersublevels are formed by the lateral electrical confinement applied on quantum wells and the transitions between them can be strongly tuned by the confinement. Under normal incidence, the peak detection wavelengths can be tuned from $\sim$50 to $\sim$90 μm (6.0 to $\sim$3.3 THz) with a gate voltage range of -5 to -2 V. The peak absorption coefficient of detection is in the order of 10^3 cm^{-1} at 77 K, and the peak detectivity of the photodetector can reach $\sim$$10^9$ cm^2 Hz$^{1/2}$ W^{-1}. The proposed approach has the advantage of forming a high uniformity of QD effective sizes and provides an alternative way to detect terahertz radiation.

(Some figures in this article are in colour only in the electronic version).

1. Introduction

The terahertz region, loosely defined as the range of frequencies from 1 to 10 THz [1], has potential applications in many areas, such as chemical sensing, medical imaging and free-space optical communications [2, 3]. With the demonstration of terahertz sources [4, 5], it is necessary to develop detection technologies in the terahertz region. Currently terahertz light can be detected by coherent or incoherent techniques, such as Schottky diode mixers, nonlinear optical crystals, photoconductive antennas and pyroelectric crystals [6–8]. However, these techniques either need sophisticated instrumentation or are slow to operate. More recently, quantum well infrared photodetectors (QWIPs) [9] and quantum dot infrared photodetectors (QDIPs) [10] have also been applied to detect terahertz wavelengths using intersubband or intersublevel transitions. Compared with QWIPs, QDIPs show more advantages, including intrinsic sensitivity to normal-incidence light, longer lifetime of photo-excited carriers and lower dark current due to the three-dimensional quantum confinement of quantum dots (QDs) [11]. Therefore, QDIPs promise to be a better candidate for the application of terahertz detection. However, current QDIPs still show low performance and one of the primary suspects for the low performance is QD size nonuniformity [12].

Here, we demonstrate a voltage tunable QDIP to detect electromagnetic radiation in the terahertz region. The proposed photodetector applies a lateral electrical confinement on quantum wells and forms a quantum disc in the quantum well region. The lateral two-dimensional quantum confinement combined with the longitudinal confinement by quantum barriers forms a QD. Using the energy states and intersublevel energy spacing in the dot formed by electrical confinement, the photodetector can be used to detect the terahertz region. Changing the confinement voltage, the intersublevel energy spacing can also be tuned and hence different wavelengths detection can be achieved. Our model shows that the peak wavelength in the absorption spectrum of the photodetector changed from $\sim$3.3 to $\sim$6 THz with a gate voltage being applied from -2 to -5 V. Moreover, changing the injection voltage of the detector leads to an even broader range up to 12.5 THz. Compared with the QDs formed by self-assembled growth, the QDs here have a higher uniformity in the effective size, due to the well-defined electrical confinement.

2. Device structure

A schematic picture of the proposed photodetector structure is shown in figure 1(*a*). The top contact is the injector, and the gate contact surrounding the injector induces the lateral
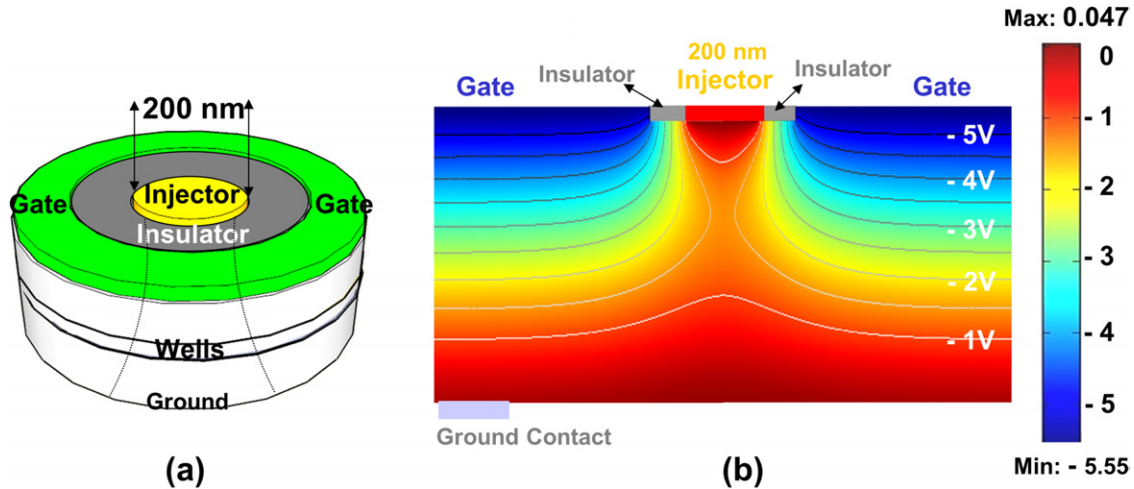
Figure 1. (*a*) Schematic picture of the QD photodetector device structure, (*b*) electrostatic potential distribution and isotropic contour curves in the structure under the gate voltage of −5 V.

electrical confinement on the quantum wells below. Between the gate and top contacts, there is an electrical insulator. The diameter of the top contacts is designed to be 200 nm. Each effective QD has a top contact, and all the gate contacts are connected to each other. When a negative voltage is applied on the gate contact, electrons are confined into the central region below the injector, while they are also confined in the quantum wells by quantum barriers. The density of states in the quantum well splits into discrete states forming intersublevels. Depending on the gate voltages, different confinements can be applied and hence different effective QD sizes can be achieved. Therefore, the intersublevel spacing in the dot can be tuned by the gate voltage. In practice, fabrication of the proposed photodetector requires a fast and economical method to generate highly dense and uniform nanoholes over large areas. Fortunately emerging high-throughput methods such as nanoimprint lithography [13] and super lens lithography [14–16] are able to meet the above requirements.

3. Results and analysis

We used 3D finite-element-method (FEM) simulations to calculate the potential distributions inside the device using Poisson and continuity equations as shown in figure 1(*b*). The gate voltage applied was −5 V. The simulated structure includes a surrounding gate contact on the top (30 nm thickness of InGaAs with an acceptor doping density of 5×10^{17} cm^{-3}), a top contact layer (50 nm thickness of InGaAs with a donor doping density of 5×10^{16} cm^{-3}), quantum well active layers consisting of InGaAs and InAlAs (thickness of 300 nm with an average donor doping density of 3.5×10^{16} cm^{-3}, one period of the quantum well including 5 nm n-doped InGaAs and 20 nm undoped InAlAs) and a bottom layer of InGaAs as ground contact. The contour curves show the isotropic potentials from −5 to −1 V. The electrical potentials push all the electrons into the nano-channel below the injector and form a two-dimensional quantum confinement.

Using the potential distribution formed by the gate voltage, we solved the three-dimensional Schrödinger equation to get the electronic states in the QD using 3D FEM. The effective mass approximation was applied to the Schrödinger equation in the cylindrical coordinates. The equation can be written as [17]

$$-\frac{\hbar^2}{2m^*}\left[\frac{1}{r}\frac{\partial}{\partial r}\left(r\frac{\partial}{\partial r}\right) + \frac{1}{r^2}\frac{\partial^2}{\partial \theta^2} + \frac{\partial^2}{\partial z^2}\right]\psi(r,\theta,z)$$
$$+ V(r,z)\psi(r,\theta,z) = E\psi(r,\theta,z) \quad (1)$$

with $V(r,z)$ the potentials obtained from above. In our model, we considered the effect of the effective mass as a function of the energy levels [18], so we kept updating the effective mass with the energy solution until the solution was almost unchanged. With different gate voltages, different potentials are effectively applied to the quantum wells as shown in figure 2(*a*). The parabolic potentials confine the electrons in the centre area and split the continuous energy band into separate energy levels. The absolute effective potential values at the centre are not valuable for the confinement, while the change in the potentials in the radial distance is important for the confinement. The main effects caused by the electrical confinement are (1) a pronounced blue shift of the energy levels in the dot, (2) the tunable intersublevel energy spacing and (3) the reduction in homogeneously broadened absorption. The intersubband selection rules in the quantum wells would not be satisfied because the carriers are being confined in both the transverse plane and the longitudinal direction. Figure 2(*b*) shows the first four wavefunction states s, p, d and f, formed by the parabolic wells as a function of the gate voltages. The full width at half maximum (FWHM) of the ground state wavefunction is in the order of ∼20 nm. With a more negative voltage, the energy states blue shift further because of the reduction in QD effective sizes. Figure 2(*c*) shows the intersublevel spacing between the adjacent energy levels at different gate voltages. It clearly demonstrates a tunable energy spacing ranging between ∼16 and ∼28 meV.
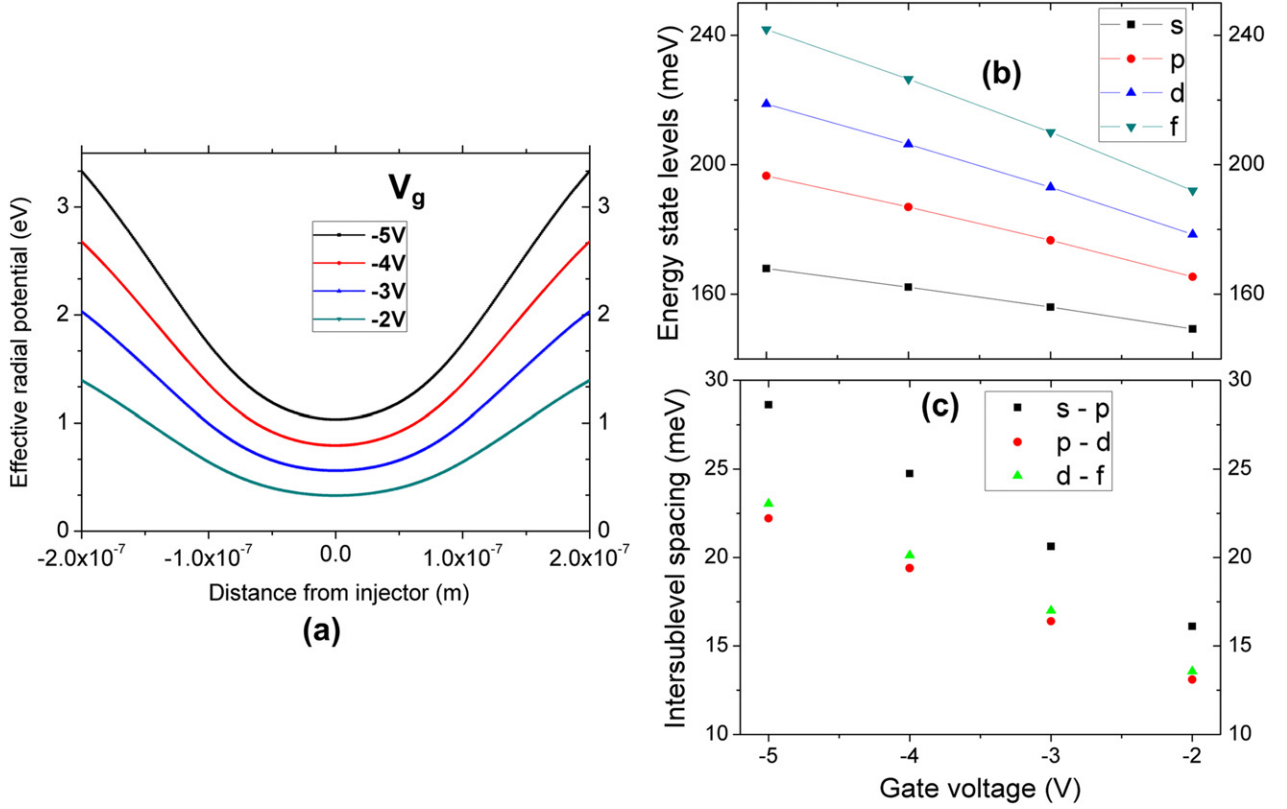
Figure 2. (*a*) The effective radial potential in the central quantum well as a function of the radial distance from the injector centre, (*b*) the positions of s, p, d, and f states as a function of the gate voltages and (*c*) the intersublevel energy spacing between the adjacent states.

The coefficient of transverse optical photon absorption, which corresponds to the normal (s-polarized) incidence for intersubband transitions, can be written as [19]

$$\alpha\left(\hbar\omega\right) = \eta\left(\frac{\omega}{n_{\text{r}}c\varepsilon_0}\right)\frac{2}{V_{\text{dot}}}\sum_{i,j}\frac{\left|e\cdot\hat{u}_{i,j}\right|^2\left(\Gamma/2\right)}{\left(E_j - E_i - \hbar\omega\right)^2 + \left(\Gamma/2\right)^2}$$
$$\times\left(f_j' - f_i'\right),\tag{2}$$

where η is the fill factor considering the spacing area between QDs, n_{r} is the average refractive index, V_{dot} is the QD volume (the factor of 2 is considering the electrons spin degeneracy), $\hat{u}_{i,j}$ is the transverse optical dipole moment values, Γ is the full width at half maximum (FWHM) of the absorption broadening (here it is mainly caused by inhomogeneous broadening) and f' is the Fermi–Dirac distribution function. The optical dipole moment for bound-to-bound transitions in the conduction band is $\hat{u}_{i,j} = \langle\Psi_i|e\hat{r}|\Psi_j\rangle$, which was evaluated by using the wavefunction solutions above. The fill factor η is ~0.145 if the dots are hexagonally distributed and the period is 500 nm. The QD volume is $V_{\text{dot}} = \frac{1}{4}\pi d^2 h$, where d is the diameter of the injector 200 nm and h is the one period thickness of quantum wells considering 25 nm. Since we are mainly considering the broadening due to inhomogeneous broadening under quasi-parabolic potential, Γ can be written as $\Gamma = 4\xi E_n$ [20], where ξ is the size deviation and E_n is the nth eigenstate level. We used a size deviation of 1% corresponding to a deviation of 2 nm for 200 nm diameter of nanoholes, which is quite

possible with current lithographic techniques. The absorption coefficient spectrum for the tunable QDs at $T = 77$ K with injection voltage $V_{\text{a}} = 0$ V is shown in figure 3(*a*). The transitions in the absorption curve are transverse bound-to-bound which are sensitive to normal-incidence light. The temperature T and Γ decide the sharpness of the absorption curve, and the carrier concentration and density of dots decide the intensity of the absorption. The density of QDs in our case is about 4.62×10^8 cm^{-2}, which is lower than that of the self-assembled dots in the range of 10^{10} cm^{-2} [21]. However, the density of the QDs can be further improved by reducing the QD array period. Changing the injection voltage V_{a}, the detection wavelengths can be further tuned to a higher terahertz range. Figure 3(*b*) shows the absorption spectrum under different gate voltages with an injection voltage V_{a} of 5 V at 77 K. Because of the injection voltage, the parabolic well in the quantum well region becomes steeper, and the detection region blue shifts. The peak detection wavelength at $V_{\text{g}} = -5$ V can now reach ~12.5 THz.

For the dark current calculations inside the photodetector, it mainly consisted of two components. The first component is due to the carriers tunnelling out of the occupied states and being excited to the band edge, and the other one is from the process of carriers' thermal excitation to the continuum. Using the Fowler–Nordheim tunnelling model, the tunnelling escape current J_{t} and the band escape thermionic current J_{b} can be

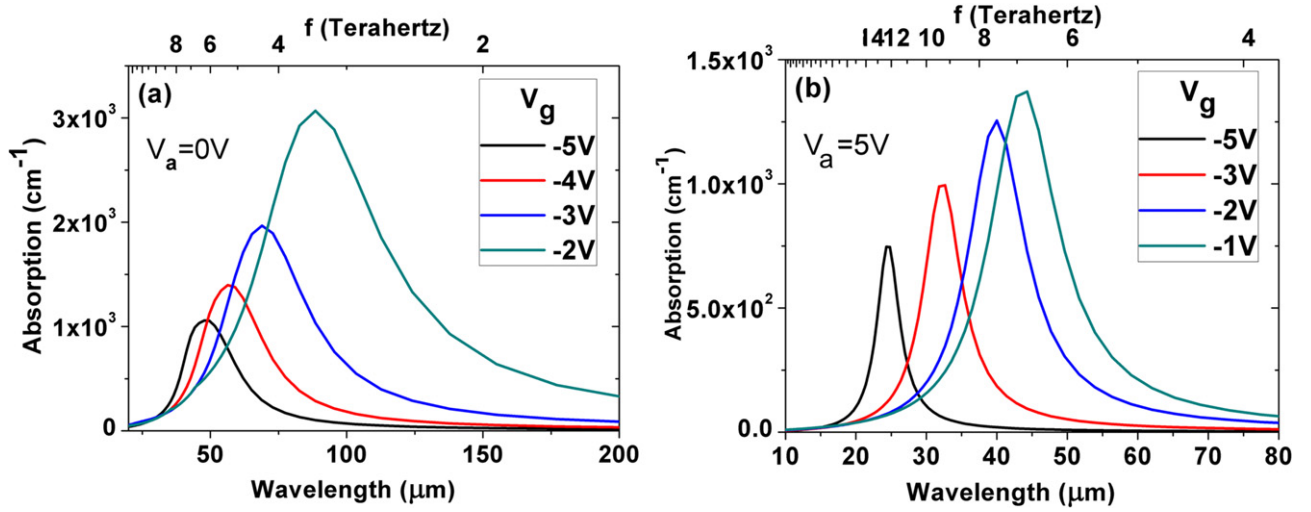J. Phys. D: Appl. Phys. **43** (2010) 155101

W Wu *et al*

Figure 3. Normal-incidence absorption coefficient for the electrical tunable QDs, (*a*) the injection voltage $V_a = 0$ V, (*b*) the detection wavelength blue shifts with an injection voltage of $V_a = 5$ V. (Colour online.)

written as [22]

$$J_t = q \frac{\mu F \tau}{L \left[1 + (uF/v_{sat})^2\right]^{1/2}} \times \frac{N d_b}{L} \times \frac{m^*}{\pi \hbar^2}$$

$$\times \int_{E_1}^{E_c} f(E) \left(\frac{\gamma E}{h}\right)$$

$$\times \exp\left[-\frac{4}{3}\left(\frac{2m_b^*}{\hbar}\right)^{1/2} \frac{(E_c - \gamma E)^{3/2}}{qF}\right] dE, \quad (3)$$

$$J_b = q \frac{\mu F}{\left[1 + (uF/v_{sat})^2\right]^{1/2}} \times \frac{N}{2\pi^2} \times \left(\frac{2m^*}{\hbar^2}\right)^{3/2}$$

$$\times \int_{E_c}^{\infty} \sqrt{E} f(E) \, dE, \quad (4)$$

where m^* is the well effective mass $= 0.041 m_0$, N is the number of quantum wells ~ 12, d_b is the barrier length $= 20$ nm, active layer thickness $L = 300$ nm, μ is the barrier mobility $= 1$ m^2 V^{-1} s^{-1}, F is the applied electric field, v_{sat} is the electron's saturation velocity $= 10^6$ m s^{-1}, E_1 is the ground energy level, E_c is the conduction band offset, $f(E)$ is the Fermi–Dirac distribution function, γE is the effective planar energy, m_b is the barrier effective mass $= 0.075 m_0$ and τ is the carrier lifetime. Normally, τ in QDIP can be in the range of nanoseconds, much bigger than that in QWIP because of the 'phonon bottleneck' considerably reducing the electron–phonon scattering [12]. However, in our case the energy level separation is small because of the operation of the photodetector in the terahertz range, so we still assume the value of τ in the range of that in QWIPs, ~ 10 ps [23]. We also assume a carrier with planar energy can use all the energy for tunnelling out in the z-direction, so $\gamma = 1$. The noise current I_n can be expressed as

$$I_n = \sqrt{4q g \Delta f I_d}, \quad (5)$$

where g is the gain of the detector, Δf is the noise bandwidth (here taken as 1 Hz) and I_d is the dark current (assuming the

area of the detector A is $400 \times 400 \, \mu\text{m}^2$). g in QDIP is generally defined as the ratio of the carrier lifetime to carrier transit time, τ/τ_{tr}, where τ_{tr} is the transit time across the effective region [24]. The saturated gain value for QDIPs can be very big due to the large lifetime of carriers and high mobility on the barrier layers. However, we obtained the gain value of ~ 6 at the bias of 1 V because of the electron–phonon scattering in our band structure. The noise I_n is calculated and plotted in figure 4(*a*). A more negative gate voltage leads to a higher noise current, because the energy levels are closer to the barrier and the carriers are easier to escape.

One of the most important detector performance parameters is detectivity $D*$.

$$D^* = R_p \frac{\sqrt{A \Delta f}}{I_n},$$

$$R_p = \frac{q}{\hbar \omega} g \eta = \frac{q}{\hbar \omega} g \left[1 - \exp(-\alpha L)\right] \frac{\tau_r}{\tau_r + \tau_e}, \quad (6)$$

where $\Delta f = 1$ Hz, R_p is the peak responsivity, $\hbar \omega$ is the photon energy at peak absorption, τ_r is the recombination time, τ_e is the escape time and $\tau_r/(\tau_r + \tau_e)$ is the escape probability, which can be fitted as an exponential function of the bias [25]. The escape probability is very small for bound-to-bound transitions because the excited bound states are below the barrier. We obtained the value of ~ 0.1 when the bias reaches 1 V. The calculated results of the detectivity at different gate voltages are shown in figure 4(*b*). With an increased bias voltage, the detectivity quickly goes up and then drops back to an almost constant. The peak detectivity is almost as large as 1.7×10^9 cm Hz$^{1/2}$ W^{-1} at $V_g = -2$ V. The performance of the photodetector can be further improved more than 10 times with a reduced period of the dots array and a lower temperature operation.

4. Conclusion

We have presented an electrical method to form QDIP to detect the terahertz region. The QDs are formed by electrical
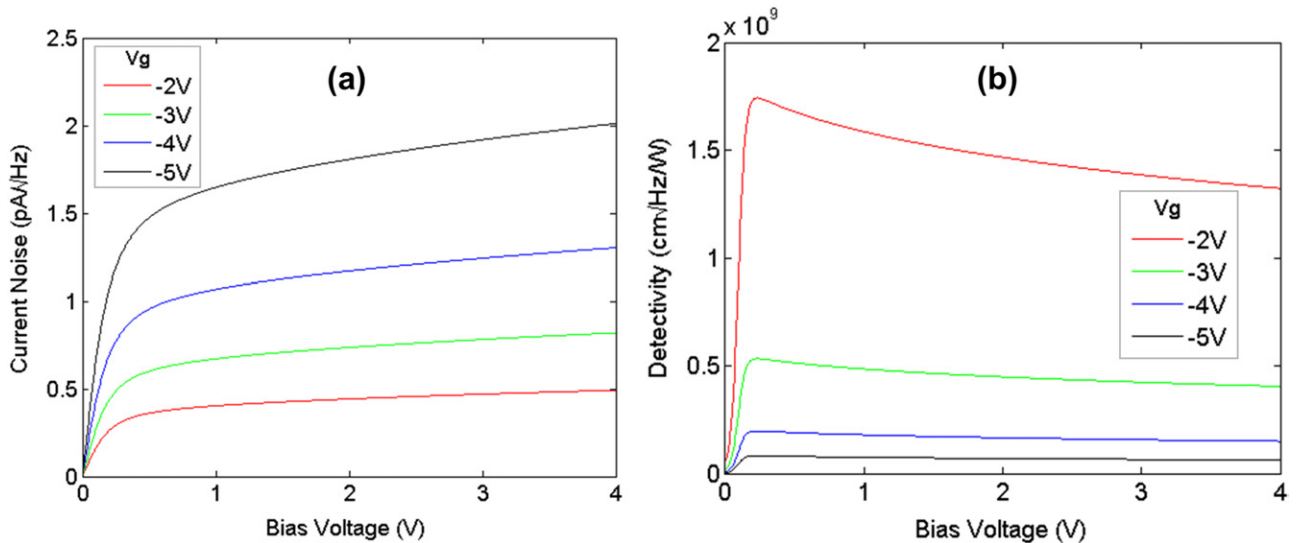
4

J. Phys. D: Appl. Phys. **43** (2010) 155101

W Wu *et al*

Figure 4. (*a*) The current noise in the detector and (*b*) the detectivity of the detector at different gate voltages. (Colour online.)

confinements applied on quantum wells. We calculated the electrical confinements and the energy states in the dots. Using the energy levels and states, we also demonstrated the normal-incidence absorption coefficients at different gate voltages. Our results show the absorption of the detector can cover the terahertz region from ∼3.3 up to ∼12.5 THz with a reasonable detectivity. With improved fabrication of a denser QD array and a further optimal design of the band structure, the photodetector can be further improved in the performance. The biggest advantages of the proposed photodetector for terahertz detection over the self-assembled QDIPs are QD effective size uniformity and the tunable wavelength detection by changing voltage.

References

[1] Kohler R, Tredicucci A, Beltram F, Beere H E, Linfield E H, Davies A G, Richie D A, Iotti R C and Rossi F 2002 Terahertz semiconductor-heterostructure laser *Nature* **417** 156–9

[2] Han P Y, Cho G C and Zhang X C 2000 Time-domain transillumination of biological tissues with terahertz pulses *Opt. Lett.* **25** 242–4

[3] Mittleman D M, Jacobsen R H and Nuss M C 1996 T-ray imaging *IEEE J. Sel. Top. Quantum Electron.* **2** 679

[4] Betz A L, Boreiko R T, Williams B S, Kumar S, Hu Q and Reno J L 2005 Frequency and phase-lock control of a 3 THz quantum cascade laser *Opt. Lett.* **30** 1837–9

[5] Williams B S, Kumar S, Callebaut H, Hu Q and Reno J S 2003 Terahertz quantum-cascade laser operating up to 137 K *Appl. Phys. Lett.* **83** 5142–4

[6] Auston D H, Cheung K P and Smith P R 1984 Picosecond photoconducting Hertzian dipoles *Appl. Phys. Lett.* **45** 284–6

[7] Brener I, Dykaar D, Frommer A, Pfeiffer L N, Lopata J, Wynn J, West K and Nuss M C 1996 Terahertz emission from electric field singularities in biased semiconductors *Opt. Lett.* **21** 1924–6

[8] Cai Y, Brener I, Lopata J, Wynn J, Pfeiffer L and Federici J 1997 Design and performance of singular electric field

terahertz photoconducting antennas *Appl. Phys. Lett.* **71** 2076–8

[9] Liu H C, Song C Y, SpringThorpe A J and Cao J C 2004 Terahertz quantum-well photodetector *Appl. Phys. Lett.* **84** 4068–70

[10] Su X H, Yang J, Bhattacharya P, Ariyawansa G and Perera A G U 2006 Terahertz detection with tunneling quantum dot intersublevel photodetector *Appl. Phys. Lett.* **89** 031117

[11] Campbell J C and Madhukar A 2007 Quantum dot infrared photodetector *Proc. IEEE* **95** 1815–27

[12] Phillips J 2002 Evaluation of the fundamental properties of quantum dot infrared detectors *J. Appl. Phys.* **91** 4590–4

[13] Chou S Y, Krauss P R and Renstrom P J 1996 Nanoimprint lithography *J. Vac. Sci. Technol.* B **14** 4129–33

[14] Wu W, Katsnelson A, Memis O G and Mohseni H 2007 A deep sub-wavelength process for the formation of highly uniform arrays of nanoholes and nanopillars *Nanotechnology* **18** 485302

[15] Wu W, Dey D, Katsnelson A, Memis O G and Mohseni H 2008 Large areas of periodic nano-holes perforated in multi-stacked films produced by lift-off *J. Vac. Sci. Technol.* B **26** 1745–7

[16] Wu W, Dey D, Memis O G, Katsnelson A and Mohseni H 2008 Fabrication of large area periodic nanostructures using nanosphere photolithography *Nanoscale Res. Lett.* **3** 351–4

[17] Wojs A, Hawrylak P, Fafard S and Jacak L 1996 Electronic structure and magneto-optics of self-assembled quantum dots *Phys. Rev.* B **54** 5604–8

[18] Kotera N and Tanaka K 2006 Determination of electron effective mass from optical transition energy in InGaAs/InAlAs quantum wells *Physica* E **32** 199–202

[19] Hoffman E H and Chuang S L 2004 Theory for intersubband absorption in quantum dots *Proc. SPIE* **5349** 90–4

[20] Wu W Y, Schulman J N, Hsu T Y and Efron U 1987 Effect of size nonuniformity on the absorption spectrum of a semiconductor quantum dot system *Appl. Phys. Lett.* **51** 710–2

[21] Schneider H and Liu H C 2006 *Quantum Well Infrared Photodetectors: Physics and Applications* (Berlin: Springer)

[22] Gin A, Movaghar B, Razeghi M and Brown G J 2005 Infrared detection from GaInAs/InP nanopillar arrays *Nanotechnology* **16** 1814–20

[23] Levine B F 1993 Quantum well infrared photodetectors *J. Appl. Phys.* **74** R1–R81

[24] Kochman B, Stiff-Roberts A D, Chakrabarti S, Phillips J D, Krishna S , Singh J and Bhattacharya P 2003 Absorption, carrier lifetime, and gain in inas-gaas quantum-dot infrared photodetectors *IEEE J. Quantum Electron.* **39** 459–67

[25] Lim H, Movaghar B, Tsao S, Taguchi M, Zhang W, Quivy A A and Razeghi M 2006 Gain and recombination dynamics of quantum-dot infrared photodetectors *Phys. Rev.* B **74** 205321